Multiple scattering of light in shock compression experiments FREE

J. A. Don Jayamanne ✉; J. R. Burie; O. Durand; R. Pierrat; R. Carminati

View Online   Export Citation

Articles You May Be Interested In

Recovering particle velocity and size distributions in ejecta with photon Doppler velocimetry

J. Appl. Phys. (August 2024)

Using ejecta measurement simulations to predict real-life results

Scilight (August 2024)

Simultaneous application of photon Doppler velocimetry and coherent backscattering for probing ejecta from shock-loaded samples

J. Appl. Phys. (September 2022)

AIP Publishing

Multiple Scattering of Light in Shock Compression Experiments

J.A. Don Jayamanne,[1, 2, a)] J.-R. Burie,[1, b)] O. Durand,[1] R. Pierrat,[2] and R. Carminati[2, 3, c)]

[1]*CEA DIF, Bruyères-le-Châtel, 91297 Arpajon Cedex, France*
[2]*Institut Langevin, ESPCI Paris, PSL University, CNRS, 75005 Paris, France*
[3]*Institut d'Optique Graduate School, Paris-Saclay University, 91127 Palaiseau, France*

[a)]Corresponding author: jerome.don-jayamanne@espci.psl.eu
[b)]jean-rene.burie@cea.fr
[c)]remi.carminati@espci.psl.eu

Abstract. Photon Doppler Velocimetry (PDV) is ubiquitous to characterize ejecta in shock physics experiments. This technique accurately measures particle velocity thanks to the induced Doppler shift, assuming light is scattered once. Nonetheless, experimental and numerical works have shown the presence of multiple scattering in shock ejecta. In order to account for multiple scattering, we develop a theoretical framework where, considering the time scales at stake, we prove that the PDV spectrogram is linked to the specific intensity of the scattered field. This specific intensity is shown to obey a Radiative Transfer Equation (RTE), which includes multiple scattering, that we generalize to take into account both Doppler shifts and statistical inhomogeneities of the ejecta in particle velocity, number density and size. We numerically solve this RTE for a realistic ejecta to compute spectrograms at different wavelengths. First, this study proves the presence of the multiple scattering regime at all studied wavelengths. Second, we show that the evolution of spectrograms on wavelength is mostly due to differences in absorption.

INTRODUCTION

Shocking a material with high explosive puts its free surface in motion while also releasing an ejecta - a cloud of fast particles traveling in front of it. While it has been shown that ejecta is caused by surface imperfections of machined materials [1-2], ejecta characterization has been an ongoing subject ever since [3]. In this effort, Photon Doppler Velocimetry (PDV) has been widely used thanks to its ability to simultaneously measure the velocities of several targets, and to its good compromise between a fine temporal resolution and a broad range of accessible velocities [4-5]. Current PDV signal analysis assumes light is scattered only once when in practice ejecta thicknesses often exceed the typical photon scattering mean-free path. Considering multiple scattering is therefore crucial for relevant experimental results analysis. Multiple scattering in ejecta has been extensively studied lately [6-13]. These approaches share the assumption that the spectrogram is in fact the specific intensity collected by the PDV probe and that this specific intensity follows a Radiative Transfer Equation (RTE) [14].

In this paper, we introduce a typical PDV setup used to characterize ejecta and explain how in the single scattering regime it accurately estimates the particle velocity distribution. Then, we establish the link between the experimental spectrogram and the specific intensity of the collected light. We present a RTE describing light transport in ejecta. Finally, we consider a realistic description of an ejecta, use an in-house Monte-Carlo simulation to solve the RTE and display the resulting simulated spectrograms at different wavelengths. This numerical study points out the appearance of the multiple scattering regime at the back of the ejecta across all wavelengths. Comparing the spectrograms at different wavelengths, they differ from one to two orders of magnitude. We show that this gap is mainly due to differences in absorption.

SPECTROGRAMS IN THE SINGLE SCATTERING REGIME

A PDV setup, as seen in Fig. 1(a), is based on a Michelson interferometer [4-5]. A probe is used to shine light, at frequency ω_0, towards an ejecta where this light gets scattered. Due to the velocity of the objects, the scattered light is slightly shifted in frequency and a portion of it is collected by the probe. The light from the measuring arm then interferes with a reference arm to create a beating signal at the photodiode. This detected signal can be written

$$\mathscr{I}(t) = \int 2\,\mathrm{Re}\left[\bar{E}_s(\mathbf{r},t)\bar{E}_0^*(\mathbf{r},t)\right]\mathrm{d}\mathbf{r}, \tag{1}$$

where $\mathrm{d}\mathbf{r}$ denotes the integration over the detector surface, $\bar{E}_s(\mathbf{r},t)$ is the analytic signal describing the scattered field and $\bar{E}_0(\mathbf{r},t)$ is the analytic signal of the reference field. In post-processing, a Short Term Fourier Transform (STFT) is applied to this signal defining the spectrogram $S(t,\omega)$ as

$$S(t,\omega) = \left| \int \mathscr{I}(\tau)w(\tau-t)\exp(i\omega\tau)\mathrm{d}\tau \right|^2 , \tag{2}$$

where $w(t)$ is a time window function [15] centered at $t=0$ and of typical width T_w. The normalization convention gives $\int w(t)\mathrm{d}t = T_w$. In the single scattering regime, making use of the far-field and scalar approximations, for a number of particle $N(t)$, the scattered fields reads

$$\bar{E}_s(\mathbf{r},t) = \frac{e^{ik_0 r}}{r} \sum_{j=1}^{N(t)} \mathscr{A}_j(\mathbf{u},\mathbf{u_0},t)\exp\left\{ -i\left[\omega_0 + k_0(\mathbf{u}-\mathbf{u_0})\cdot\mathbf{v}_j(t)\right]t \right\} , \tag{3}$$

where ω_0 is the optical frequency, $k_0 = \omega_0/c$ with c the light velocity in vacuum, $\mathbf{u_0}$ is the direction of illumination, $\mathbf{u} = \mathbf{r}/|\mathbf{r}|$ is the direction of observation, $\mathscr{A}_j(\mathbf{u},\mathbf{u_0},t)$ is the amplitude of the field scattered by particle j and $\mathbf{v}_j(t)$ its velocity. Using Eq. (3) and that the observation directions $\mathbf{u} = -\mathbf{u_0}$, the spectrogram given in Eq. (2) becomes

$$S(t,\omega) \simeq \frac{\pi^2 |\mathscr{A}_0|^2}{r^2} \int \sum_{j=1}^{N(t)} |\mathscr{A}_j(-\mathbf{u_0},\mathbf{u_0},t)|^2 \left\{ \left| \delta\left[\omega + \frac{4\pi}{\lambda}v_j(t)\right] \right|^2 + \left| \delta\left[\omega - \frac{4\pi}{\lambda}v_j(t)\right] \right|^2 \right\} \mathrm{d}\mathbf{r} , \tag{4}$$

where $\mathscr{A}_0$ is the amplitude of the reference field and δ the Dirac delta function. This simple expression allows one to convert the frequency appearing in PDV spectrograms directly into a velocity as shown in Fig. 1(b).
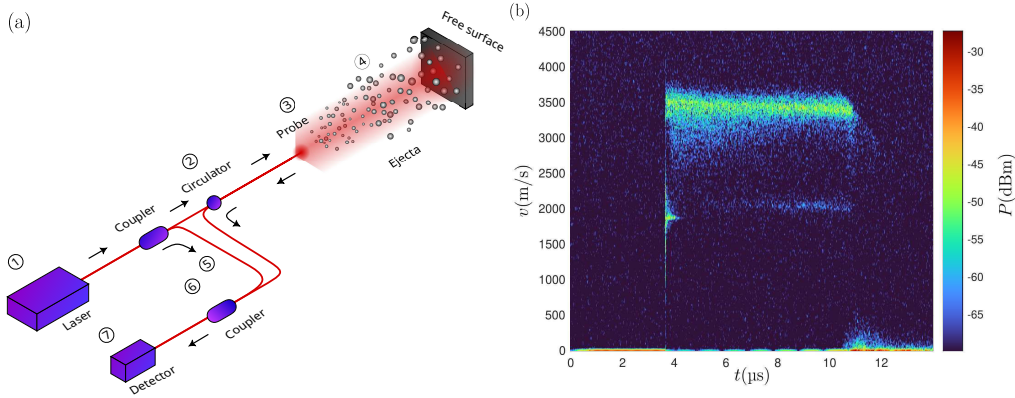

FIGURE 1. (a) Typical PDV setup. The probe illuminates the ejecta and the free surface with a highly collimated laser beam (numerical aperture of 4.2 mrad and pupil size $\phi_p = 1.3\,\mu\text{m}$). Light is then scattered before being collected back by the same probe. Due to the object's velocity, the scattered light is shifted in frequency. It then interferes at the detector with the light from the reference arm, creating a beating signal. (b) Spectrogram of a tin micro-jetting experiment under pyrotechnic shock at $P = 25\,\text{GPa}$. The tin sample was engraved with $25\,\mu\text{m} \times 8\,\mu\text{m}$ grooves. Independent Asay window measurements gave an estimated surface mass $M_s = 5\,\text{mg/cm}^2$.

The approach above relies on the single scattering hypothesis. In a statistically homogeneous medium of longitudinal size L, this approximation holds as long as the optical thickness $b(\omega_0) = L/\ell_s(\omega_0) \ll 1$, where $\ell_s(\omega_0)$ is the light scattering mean-free path. In a medium where the statistical properties as the number density or the size distribution of the particles depend on position, the condition becomes

$$b(\omega_0) = \int \frac{\mathrm{d}z}{\ell_s(z,\omega_0)} \ll 1 , \tag{5}$$

where $\ell_s(z,\omega_0)$ is the inhomogeneous scattering mean-free path at position z along ejection axis. In many experiments [7, 16-17] the optical thickness far exceeds unity. In the typical ejecta described later in this paper, we found $b(\omega_0) = 42$ which corresponds to the deep multiple scattering regime. The single scattering description for light transport in ejecta is therefore unsatisfactory and a quantitative analysis requires the derivation of a theoretical model to take into account multiple scattering.

SPECTROGRAMS IN THE MULTIPLE SCATTERING REGIME

To account for multiple scattering in PDV measurements, the RTE appears as a natural tool. Since it is a transport equation for the specific intensity [18-21], we first need to link the latter to the experimental spectrogram. In statistical optics, the specific intensity $I(\mathbf{r},\mathbf{u},t,\omega)$ is defined as

$$\delta(k-k_R)I(\mathbf{r},\mathbf{u},t,\omega) = \int \left\langle \bar{E}\left(\mathbf{r}+\frac{\rho}{2},t+\frac{\tau}{2}\right)\bar{E}^*\left(\mathbf{r}-\frac{\rho}{2},t-\frac{\tau}{2}\right)\right\rangle \exp(-ik\mathbf{u}\cdot\rho+i\omega\tau)\mathrm{d}\rho\mathrm{d}\tau, \qquad (6)$$

where $\bar{E}(\mathbf{r},t)$ is the analytical signal of the field and $k_R = n_{\text{eff}}\omega_0/c$ with n_{eff} the real part of the effective refractive index. As the STFT used to define the spectrogram, the above relation performs a time-frequency analysis but based on a different tool, the Wigner transform. It also makes use of of a statistical average over all configurations of disorder denoted by $\langle\cdot\rangle$. A key point to establish the link between the spectrogram and the specific intensity is to have the different time scales involved in an ejecta experiment several orders of magnitude apart. More precisely, the condition is $T_0 \ll T_d \ll \delta T \ll T_w \ll T_c$ where respectively T_0 is the period of the source field $\bar{E}_0$, T_d the time corresponding to the bandwidth of the digitizer, δT the time scale of the typical Doppler shifts, T_w is the width of the STFT window and T_c the characteristic time of evolution in the statistical properties of the cloud. Typically in shock experiments, we have $T_0 = 1\times10^{-15}\,\text{s}$, $T_d = 1\times10^{-10}\,\text{s}$, $\delta T = 1\times10^{-9}\,\text{s}$, $T_w = 1\times10^{-8}\,\text{s}$ and $T_c = 1\times10^{-6}\,\text{s}$, which satisfies the previous condition.

Leveraging this property and invoking ergodicity to replace the statistical average present in Eq. (6) by a time average over the window of Fourier analysis T_w, a generalization of Eq. (4) to the multiple scattering regime can be written

$$\delta(k-k_R)S(t,\omega) = T_w|\mathscr{A}_0|^2 \int_G [I_s(\mathbf{r},\mathbf{u},t,\omega_0+\omega)+I_s(\mathbf{r},\mathbf{u},t,\omega_0-\omega)]\,\mathbf{u}\cdot\mathbf{n}\mathrm{d}\mathbf{u}\mathrm{d}\mathbf{r}, \qquad (7)$$

where G is the etendue of the detector (surface of detection and angular aperture), $\mathrm{d}\mathbf{u}$ corresponds to integration over the solid angle, and $\mathbf{n}$ is the normal to the detector surface. Since the probing beam is not in the etendue of the detector, it will not be collected by the probe and will not contribute to the spectrogram. Without loss of generality, the scattered specific intensity I_s can therefore be replaced by the full specific intensity I in Eq. (7). We see that this formulation keeps the structure of the Eq. (3) while depending on the specific intensity which is the appropriate quantity to describe light propagation in a scattering medium. This relation rigorously proves the link between the PDV spectrogram and the specific intensity. To simulate a spectrogram, one now needs to establish a transport equation for the specific intensity.

QUASI-HOMOGENEOUS AND INELASTIC RADIATIVE TRANSFER EQUATION

In the previous section, we have shown that simulating a spectrogram is equivalent to computing the specific intensity scattered by an ejecta. What deter us from using the usual form of the RTE is that we have to account for both spatio-temporal statistical inhomogeneities of the medium and inelastic scattering caused by the motion the scatterers. We have shown from first principles of wave scattering and multiple scattering theory [19-22] that the specific intensity in an ejecta of spherical particles follows a quasi-homogeneous and inelastic RTE [23-24]. The novelty of this work resides in the definition of a generalized phase function describing inelastic scattering and in the subtle detail that all the quantities appearing in the RTE depends on both position $\mathbf{r}$ and time t. This last feature was made possible by doing a quasi-homogeneous approximation [25] on the statical properties of the ejecta. The resulting equation takes the form

$$\left[\frac{1}{v_E(\mathbf{r},t,\omega)}\frac{\partial}{\partial t}+\mathbf{u}\cdot\nabla_\mathbf{r}+\frac{1}{\ell_e(\mathbf{r},t,\omega)}\right]I(\mathbf{r},\mathbf{u},t,\omega) = \frac{1}{\ell_s(\mathbf{r},t,\omega)}\int p(\mathbf{r},\mathbf{u},\mathbf{u}',t,\omega,\omega')I(\mathbf{r},\mathbf{u}',t,\omega')\mathrm{d}\mathbf{u}'\frac{\mathrm{d}\omega'}{2\pi}. \qquad (8)$$

The extinction mean-free path ℓ_e is defined as

$$\frac{1}{\ell_e(\mathbf{r},t,\omega)} = \rho(\mathbf{r},t)\int \sigma_e(a,\omega)h(\mathbf{r},t,a)\mathrm{d}a, \qquad (9)$$

where $\sigma_e(a,\omega)$ is the extinction cross-section of a particle with radius a at frequency ω and $h(\mathbf{r},t,a)$ is the probability density at position $\mathbf{r}$ and time t of having a particle with radius a. The scattering mean-free path ℓ_s and the phase

function p are defined as

$$\frac{1}{\ell_s(\mathbf{r},t,\omega)}p(\mathbf{r},\mathbf{u},\mathbf{u}',t,\omega,\omega') = \rho(\mathbf{r},t)\int\frac{\mathrm{d}\sigma_s(a,\mathbf{u}\cdot\mathbf{u}',\omega)}{\mathrm{d}\mathbf{u}}2\pi\delta\left[\omega'-\omega-k_R(\mathbf{u}'-\mathbf{u})\cdot\mathbf{v}\right]g(\mathbf{r},t,a,\mathbf{v})\mathrm{d}a\mathrm{d}\mathbf{v}, \qquad (10)$$

where $\sigma_s(a,\omega)$ is the scattering cross-section of a particle with radius a and $g(\mathbf{r},t,a,\mathbf{v})$ is the probability density at position $\mathbf{r}$ and time t of having a particle with radius a and velocity $\mathbf{v}$. With this definition, the phase function is normalized as $\int p(\mathbf{r},\mathbf{u},\mathbf{u}',t,\omega,\omega')\mathrm{d}\mathbf{u}'\mathrm{d}\omega'/(2\pi) = 1$. Finally, v_E is the energy velocity. Since we have nonresonant scattering, the energy velocity is given by $v_E = c/n_{\mathrm{eff}}$. This equation can be understood as an energy balance. The two derivatives of the specific intensity on the left-hand side of Eq. (8) describe its spatio-temporal evolution. This evolution is driven by both losses and gains. Losses are due to absorption and scattering, this corresponds to the extinction mean-free path term on the left-hand side of Eq. (8). It is important to note that these losses happen at the same frequency ω. The gains, also due to scattering, are described by the phase function on the right-hand side of Eq. (8). This scattering process is inelastic, allowing a conversion from a frequency ω' to ω.

Simulating a spectrogram now relies on our ability to solve this RTE for a scattering medium and a geometry corresponding to a real ejecta.

NUMERICAL SIMULATIONS

To solve transport equations such as the RTE, Monte-Carlo simulations have become the global standard [26]. We implemented such a scheme for the generalized RTE described above. To compute a first spectrogram, we decided to use the simple scenario given by Shi *et al* [13], a single shock on tin. The resulting ejecta is assumed to be a cloud of spherical particles in a 3-D slab geometry with a perfectly specular reflective free surface at the back. The statistical parameters therefore vary only on z, the ejecta direction. We assume a lognormal particle size distribution [27]

$$h(a) = \frac{1}{a\sigma\sqrt{2\pi}}\exp\left[-\frac{(\ln a - \mu)^2}{2\sigma^2}\right], \qquad (11)$$

where $\mu = \ln(\mu_a^2/\sqrt{\mu_a^2+\sigma_a^2})$ and $\sigma^2 = \ln(1+\sigma_a^2/\mu_a^2)$, μ_a and σ_a being, respectively, the mean and standard deviation of the particle size distribution. Since this is a single shock in vacuum, position and velocity are linearly linked as $z = vt$ with t being time. The mass-velocity distribution is assumed to be of the form

$$M(v) = M_s\exp\left[-\beta\left(\frac{v}{v_s}-1\right)\right], \qquad (12)$$

where M_s is the total surface mass, β gives the slope of the distribution and v_s is the velocity of the free surface [28]. For numerical values, we have $\mu_a = 0.75\,\mu\mathrm{m}$, $\sigma = 0.5$ for the size distribution. The total surface mass $M_s = 20\,\mathrm{mg/cm^2}$ and the parameter $\beta = 10$. We impose minimum and maximum values for the radii and the velocities $a_{\min} = 0.1\,\mu\mathrm{m}$, $a_{\max} = 2.0\,\mu\mathrm{m}$, $v_{\min} = v_s = 2250\,\mathrm{m/s}$ and $v_{\max} = 4500\,\mathrm{m/s}$. Since all particles are spherical, we use Mie theory [29-30] to compute the corresponding cross-sections σ_s and σ_e and then the mean-free paths ℓ_s and ℓ_e. Mie theory also provides the differential scattering cross-section $\mathrm{d}\sigma_s/(\mathrm{d}\mathbf{u})$.

Figure 2 presents numerical simulations of spectrograms for a given time t in the dynamics of the ejecta. The frequencies given on the x-axis are normalized by $\omega_s = 4\pi v_s/\lambda$ the Doppler shift associated to the free surface. As an order of magnitude, each spectrum presented in Fig. 2 took 8 h of compute time on 24 48-core Xeon Gold 5220R, each clocked at 2.2 GHz. While semi-analytical methods have been used to speed up the computation, the narrow aperture of the probe means that only a fraction of the random walks are ultimately recovered. This phenomenon is the most detrimental to computation time.

First, in Fig. 2(a), we compare the spectrum given for the full Monte-Carlo simulation (blue solid line) at $\lambda_0 = 1550\,\mathrm{nm}$, and the spectrum for the same simulation where only single scattering is considered (black dashed line). For high frequencies, the single scattering spectrum matches the one with all scattering sequences. Since high frequencies corresponds to high velocities, this gives information on the ejecta's front. This result confirms that the ejecta's front is mostly in the single scattering regime. When looking at the lower frequencies, which corresponds to the low velocities and therefore the back of the ejecta, the single scattering contribution highly drops compared to the overall spectrum. As suggested by Franzkowiak *et al.* [7] and Andriyash *et al.* [6], this proves that light collected from the ejecta's back
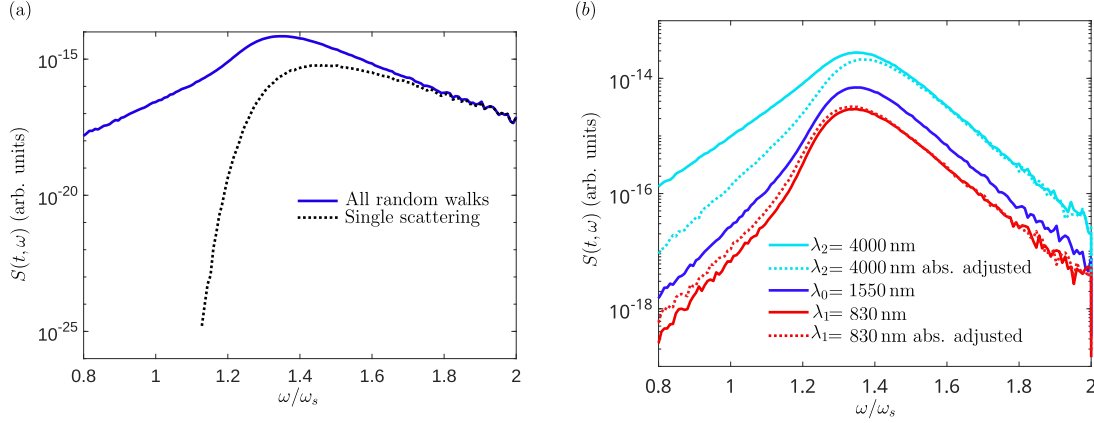
FIGURE 2. (a) Comparison between single scattering (black dashed line) and multiple scattering spectra (blue solid line) at $\lambda_0 = 1550\,\text{nm}$. The simulations are carried out with the ejecta parameters specified above and at time $t = 10\,\mu\text{s}$. (b) Comparison of spectrograms at wavelengths $\lambda_0 = 1550\,\text{nm}$ (blue solid line), $\lambda_1 = 830\,\text{nm}$ (red solid line) and $\lambda_2 = 4000\,\text{nm}$ (cyan solid line). Spectrograms at $\lambda_1 = 830\,\text{nm}$ (dashed red solid line) and $\lambda_2 = 4000\,\text{nm}$ (cyan dashed line) with adjusted absorption mean free paths the match the ones of $\lambda_0 = 1550\,\text{nm}$.

is inevitably multiply scattered. This is confirmed by the value of the optical thickness $b(\omega_0) = 42$ corresponding to this ejecta. While the resulting frequencies of multiple scattering sequences could have been completely random, they remain in the same frequency window than the single scattering ones. Taking a closer look at the scattering sequences, not displayed here, we find that the multiple scattering sequences are mostly made of one backscattering event and multiple forward scattering events. Since forward scattering yields low Doppler shifts, multiple scattering sequences have a cumulated shift corresponding to the velocity of the particle they backscattered on, with a broadening due to the forward scattering events.

Second, in a context where new wavelengths are becoming available for PDV measurements, we study the spectrogram dependence on wavelength and try to better understand it. We now consider two additional wavelengths $\lambda_1 = 830\,\text{nm}$, and $\lambda_2 = 4000\,\text{nm}$. For these additional wavelengths, at the corresponding frequencies ω_1 and ω_2, the optical thickness of the ejecta is, respectively, $b(\omega_1) = 41$ and $b(\omega_2) = 41$. At all wavelengths, the ejecta appears deep in multiple scattering regime. Since the optical thicknesses are similar, we expect the same predominance of the scattering regimes. In Fig. 2 (b), we now compare the spectrograms at the two additional wavelength, λ_1 (red solid line) and λ_2 (cyan solid line) to the one at λ_0 (blue solid line). We observe that while similar, the spectrogram has respectively a lower level at λ_1 and a higher level at λ_2 compared to λ_0. To investigate this, it is interesting to consider the anisotropy factor $\bar{g}(\omega)$ defined as

$$\bar{g}(\omega) = \int \frac{h(a)\sigma_s(a,\omega)}{\bar{\sigma}_s(\omega)} g(a,\omega)\mathrm{d}a \qquad (13)$$

where $\bar{\sigma}_s(\omega)$ is the scattering cross-section averaged on the size distribution $h(a)$ and $g(a,\omega)$ the anisotropy factor of a single particle of size a. When $\bar{g}(\omega) \approx 1$, we mostly have forward scattering, i.e., less light is collected by the probe, and when $\bar{g}(\omega) \approx -1$ we mostly have backscattering, i.e., more light is collected by the probe. For the considered frequencies, we obtain $\bar{g}(\omega_0) = 0.49$, $\bar{g}(\omega_1) = 0.55$ and $\bar{g}(\omega_2) = 0.24$. The respectively higher anisotropy for λ_1 and lower for λ_2 compared to λ_0 explains the difference in observed spectrogram levels. Nonetheless this gap widens at lower frequencies, the region of the spectrum mostly in the multiple scattering regime.

The only remaining discrepancy would be absorption. The absorption mean-free path is defined as $1/\ell_a = 1/\ell_e - 1/\ell_s$. At the back of the ejecta, the absorption mean-free path ℓ_a is, respectively $\ell_a(\omega_0) = 4.78 \times 10^{-4}\,\text{m}$, $\ell_a(\omega_1) = 4.06 \times 10^{-4}\,\text{m}$ and $\ell_a(\omega_2) = 1.30 \times 10^{-3}\,\text{m}$. To confirm that this difference explains the gap in the spectrograms, we run the simulation again at $\lambda = 830\,\text{nm}$ and $\lambda = 4000\,\text{nm}$ but artificially tuning the values of ℓ_a to be the same as for $\lambda = 1550\,\text{nm}$ thought out the ejecta. The results are displayed in dotted lines in Fig. 2 (b). This change to the absorption mean-free path allows to recover much more consistent slopes at low frequencies. This result confirms that the dependence of spectrograms on wavelengths is mainly due to differences in absorption.

CONCLUSION

In summary, we have created a model for PDV measurements in shock experiments highlighting the effect of multiple light scattering. Through the rigorous derivation of the link between the PDV spectrograms and the specific intensity, this work fills a void in the chain aiming to provide tools for the quantitative analysis of PDV measurements. The proposed quasi-homogeneous and inelastic RTE allows a better characterization of complex ejecta. We have described an application example on a realistic ejecta, where we point out the presence of the multiple scattering regime. We have shown how that this multiple scattering portion of the spectrum changes drastically depending on the wavelength. Finally, we have proven that this spectral dependence is the signature of differences in absorption.

On the applied side, this work pushes towards a complete simulation chain for shock compression experiments. Considering the available numerical tools for ejecta dynamics [31-34] and the available experimental spectrograms, such studies would be of great interest either for the development of new PDV setups or for the refinement of ejecta models. On a more fundamental level, considering the large optical thicknesses ($b > 10$) of some ejecta, a diffusion approximation of the RTE could be derived to simplify the analyses in practice. These are potential lines of research to be pursued in further studies.

ACKNOWLEDGMENTS

REFERENCES

1. J. R. Asay, L. P. Mix, and F. C. Perry, "Ejection of material from shocked surfaces," Appl. Phys. Lett. **29**, 284–287 (1976).
2. P. Andriot, P. Chapron, and F. Olive, "Ejection of material from shocked surfaces of tin, tantalum and lead-alloys," in *AIP Conference Proceeding Volume 78* (AIP, 1982) pp. 505–509.
3. W. T. Buttler, R. J. R. Williams, and F. M. Najjar, "Foreword to the Special Issue on Ejecta," J. Dyn. Behav. Mater. **3**, 151–155 (2017).
4. O. T. Strand, D. R. Goosman, C. Martinez, T. L. Whitworth, and W. W. Kuhlow, "Compact system for high-speed velocimetry using heterodyne techniques," Rev. Sci. Instrum. **77**, 083108 (2006).
5. P. Mercier, J. Benier, A. Azzolina, J. M. Lagrange, and D. Partouche, "Photonic doppler velocimetry in shock physics experiments," J. Phys. IV **134**, 805–812 (2006).
6. A. V. Andriyash, M. V. Astashkin, V. K. Baranov, A. G. Golubinskii, D. A. Irinichev, A. N. Kondrat'ev, S. E. Kuratov, V. A. Mazanov, D. B. Rogozkin, S. N. Stepushkin, and V. Y. Khatunkin, "Optoheterodyne Doppler measurements of the ballistic expansion of the products of the shock wave-induced surface destruction: Experiment and theory," J. Exp. Theor. Phys. **122**, 970–983 (2016).
7. J.-E. Franzkowiak, P. Mercier, G. Prudhomme, and L. Berthe, "Multiple light scattering in metallic ejecta produced under intense shockwave compression," Appl. Opt. **57** (2018).
8. A. V. Andriyash, M. V. Astashkin, V. K. Baranov, A. G. Golubinskii, D. A. Irinichev, V. Y. Khatunkin, A. N. Kondratev, S. E. Kuratov, V. A. Mazanov, D. B. Rogozkin, and S. N. Stepushkin, "Application of photon Doppler velocimetry for characterization of ejecta from shock-loaded samples," J. Appl. Phys. **123**, 243102 (2018).
9. A. V. Andriyash, S. A. Dyachkov, V. V. Zhakhovsky, D. A. Kalashnikov, A. N. Kondratev, S. E. Kuratov, A. L. Mikhailov, D. B. Rogozkin, A. V. Fedorov, S. A. Finyushin, and E. A. Chudakov, "Photon Doppler Velocimetry and Simulation of Ejection of Particles from the Surface of Shock-Loaded Samples," J. Exp. Theor. Phys. **130**, 338–357 (2020).
10. A. N. Kondrat'ev, A. V. Andriyash, S. E. Kuratov, and D. B. Rogozkin, "Application of multiple scattering theory to Doppler velocimetry of ejecta from shock-loaded samples," J. Quant. Spectrosc. Radiat. Transfer **246**, 106925 (2020).
11. X.-F. Shi, D.-J. Ma, S.-l. Dang, Z.-Q. Ma, H.-Q. Sun, A.-M. He, and P. Wang, "Reconstruction and interpretation of photon Doppler velocimetry spectrum for ejecta particles from shock-loaded sample in vacuum*," Chin. Phys. B **30**, 066201 (2021).
12. A. V. Andriyash, S. M. Ismailov, V. G. Kamenev, G. V. Kaplukov, A. N. Kondratev, P. V. Kubasov, S. E. Kuratov, D. B. Rogozkin, A. A. Tikhov, I. V. Tur, A. S. Shubin, S. A. Shubin, and P. N. Yaroschuk, "Simultaneous application of photon Doppler velocimetry and coherent backscattering for probing ejecta from shock-loaded samples," J. Appl. Phys. **132**, 123103 (2022).
13. X.-f. Shi, D.-j. Ma, S.-l. Dang, Z.-q. Ma, H.-q. Sun, A.-m. He, and W. Pei, "Reconstruction of ejecta field based on photon Doppler velocimetry from shock-loaded samples in vacuum," J. Quant. Spectrosc. Radiat. Transfer **282**, 108106 (2022).
14. S. Chandrasekhar, *Radiative Transfer* (Dover, New York, 1950).
15. F. Harris, "On the use of windows for harmonic analysis with the discrete Fourier transform," IEE Proc. **66**, 51–83 (1978).
16. J.-E. Franzkowiak, G. Prudhomme, P. Mercier, S. Lauriot, E. Dubreuil, and L. Berthe, "PDV-based estimation of ejecta particles' mass-velocity function from shock-loaded tin experiment," Rev. Sci. Instrum. **89**, 033901 (2018).
17. W. T. Buttler, R. K. Schulze, J. J. Charonko, J. C. Cooley, J. E. Hammerberg, J. D. Schwarzkopf, D. G. Sheppard, J. J. Goett, M. Grover, B. M. La Lone, S. K. Lamoreaux, R. Manzanares, J. I. Martinez, J. D. Regele, M. M. Schauer, D. W. Schmidt, G. D. Stevens, W. D. Turley, and R. J. Valencia, "Understanding the transport and break up of reactive ejecta," Physica D **415**, 132787 (2021).
18. Y. N. Barabanenkov, "On the spectral theory of radiation transport equations," Sov. Phys. JETP **29**, 679–684 (1969).
19. S. M. Rytov, Y. A. Kravtsov, and V. I. Tatarskii, *Principles of Statistical Radiophysics*, Vol. 4 (Springer-Verlag, Berlin, 1989).

20. L. A. Apresyan and Y. A. Kravtsov, *Radiation Transfer: Statistical and Wave Aspects* (Gordon and Breach Publishers, Amsterdam, 1996).
21. R. Carminati and J. C. Schotland, *Principles of Scattering and Transport of Light* (Cambridge University Press, 2021).
22. P. Sheng, *Introduction to Wave Scattering, Localization and Mesoscopic Phenomena* (Springer, Berlin, 2006).
23. R. Pierrat, "Transport equation for the time correlation function of scattered field in dynamic turbid media," J. Opt. Soc. Am. A **25** (2008).
24. J. G. Hoskins, J. Kraisler, and J. C. Schotland, "Radiative transport in quasi-homogeneous random media," J. Opt. Soc. Am. A **35**, 1855 (2018).
25. L. Mandel and E. Wolf, *Optical Coherence and Quantum Optics* (University Press, Cambridge, 1995).
26. R. Siegel and J. R. Howell, *Thermal radiation heat transfer*, 3rd ed. (Hemisphere, Taylor and Francis, 1992).
27. M. M. Schauer, W. T. Buttler, D. K. Frayer, M. Grover, B. M. LaLone, S. K. Monfared, D. S. Sorenson, G. D. Stevens, and W. D. Turley, "Ejected Particle Size Distributions from Shocked Metal Surfaces," J. Dyn. Behav. Mater. **3** (2017), 10.1007/s40870-017-0111-9.
28. S. K. Monfared, D. M. Oró, M. Grover, J. E. Hammerberg, B. M. LaLone, C. L. Pack, M. M. Schauer, G. D. Stevens, J. B. Stone, W. D. Turley, and W. T. Buttler, "Experimental observations on the links between surface perturbation parameters and shock-induced mass ejection," J. Appl. Phys. **116**, 063504 (2014).
29. G. Mie, "Beiträge zur Optik trüber Medien, speziell kolloidaler Metallösungen," Ann. Phys. Leipzig **25**, 377 (1908).
30. C. F. Bohren and D. R. Huffman, *Absorption and scattering of light by small particles* (Wiley, New York, 1983).
31. J. Fung, A. Harrison, S. Chitanvis, and J. Margulies, "Ejecta source and transport modeling in the FLAG hydrocode," Comput. Fluids **83**, 177–186 (2013).
32. O. Durand and L. Soulard, "Large-scale molecular dynamics study of jet breakup and ejecta production from shock-loaded copper with a hybrid method," J. Appl. Phys. **111**, 044901 (2012).
33. O. Durand and L. Soulard, "Power law and exponential ejecta size distributions from the dynamic fragmentation of shock-loaded Cu and Sn metals under melt conditions," J. Appl. Phys. **114**, 194902 (2013).
34. O. Durand and L. Soulard, "Mass-velocity and size-velocity distributions of ejecta cloud from shock-loaded tin surface using atomistic simulations," J. Appl. Phys. **117**, 165903 (2015).